A structural and theoretical study of the monolithiation of hydroxylamines [1]

David R. Armstrong [a,*], William Clegg [b,2], Susan M. Hodgson [b], Ronald Snaith [c], Andrew E.H. Wheatley [c]

[a] *Department of Pure and Applied Chemistry, University of Strathclyde, Glasgow, G1 1XL, UK*
[b] *Department of Chemistry, University of Newcastle, Newcastle upon Tyne, NE1 7RU, UK*
[c] *Department of Chemistry, University of Cambridge, Cambridge, CB2 1EW, UK*

Abstract

Dibenzylhydroxylamine, $(PhCH_2)_2NOH$, is readily monolithiated to yield an unsolvated product, **1**. In the solid state **1** is hexameric, with a core of two stacked $(OLi)_3$ rings. The metal centres are further coordinated by virtue of intra-monomer chelation using hydroxylamide *N*-centres, yielding three-membered NOLi rings. Ab initio M.O. calculations have been used to probe the structural options available for lithium hydroxylamide itself, $[H_2NOLi]_n$ ($n = 1$–4,6,8,9). The calculational findings shed light on why a hexameric structure is found in the experimental system. © 1998 Elsevier Science S.A.

*Keywords:* Ab initio calculations; Hydroxylamine; Lithium; X-ray structure

1. Introduction

A study [1] of alkoxyamidolithium amination, whereby $LiRNOR^1$ gives $LiRNR^2$ and $LiOR^1$ on reaction with LiR^2 (Scheme 1), first prompted a theoretical examination [2] of the intermediate species, which were shown to demonstrate lithium-bridging of N–O bonds. Ab initio S.C.F. M.O. modelling of the *O*- and *N*-monolithiated derivatives of hydroxylamine, H_2NOH, led to the observation that, particularly in the latter case, the N–O bond lengthened considerably from the 1.439 Å value characteristic of hydroxylamine, thus 'priming' the species for further reaction. Nevertheless, it is not until now that the existence of such chelated lithium hydroxylamides has been proven. This work reports the synthesis and structural characterisation of the first such *O*-monolithiate to demonstrate stabilisation of the metal centres not only by aggregation but also by chelation using the hydroxylamide *N*-centres. In addition, further calculations have been done in an attempt to explain the solid-state structure of the monolithiated product.

2. Results and discussion

The monolithiation of dibenzylhydroxylamine, $(PhCH_2)_2NOH$, is readily effected in toluene by the addition of one equivalent of *n*-butyllithium (Scheme 2). X-ray crystallography demonstrates that the product, **1**, is a hexamer in the solid state. Fig. 1 shows the hexameric $[(PhCH_2)_2NOLi]_6$ aggregate in its entirety while Fig. 2 displays the core, containing two stacked $(OLi)_3$ rings and six three-membered NOLi chelates. ^1H NMR spectroscopy indicates the presence of toluene in the lattice, integration suggesting a **1**:toluene ratio of

---
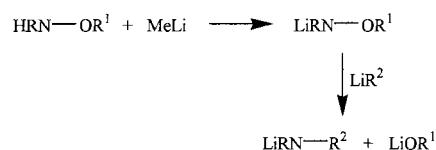
* Corresponding author.
[1] Dedicated to Professor Ken Wade on the occasion of his 65th birthday and in recognition of his outstanding and ongoing contributions to Main Group Chemistry.
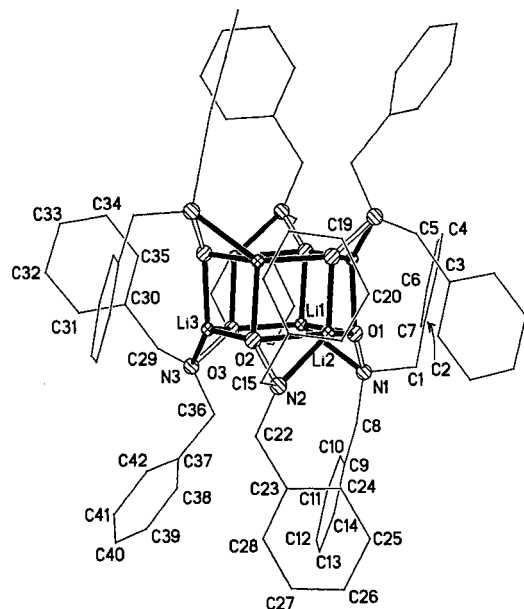[2] Also corresponding author.

$$HRN\!-\!OR^1 + MeLi \longrightarrow LiRN\!-\!OR^1$$

$$\downarrow LiR^2$$

$$LiRN\!-\!R^2 + LiOR^1$$

Scheme 1.

Fig. 1. Molecular structure of $\mathbf{1}_6 \cdot$ PhMe; hydrogen atoms and the toluene molecule are omitted for clarity.

Scheme 2.

functionality cyclises to yield six three-membered N–O–Li rings. Presumably by virtue of the interaction of benzyl residues, there are some nominal differences between the three hydroxylamide centres on each trimeric ring. This is most clearly borne out by the observation of an anomalously short Li(1)–N(1) bond (2.100(6) Å) (cf. Li(2)–N(2) = 2.137(6) Å, Li(3)–N(3) = 2.156(6) Å). One presumes that it is as a result of strain in the chelates that inter-monomer Li–O stabilisation represents the shorter of the two classes of lithium–oxygen linkage observed in either ring trimer.

7.25:1. However, X-ray crystallography indicates that the correct formulation is $\mathbf{1}_6 \cdot$ PhMe (selected bond lengths and angles are given in Table 1). The hexameric aggregate is based on two stacked (OLi)$_3$ trimeric rings (for examples of (XLi)$_6$ aggregates (X = C, N, O) see for example Ref. [3]). The Li–O interactions in each ring alternate between 'short' (1.883(6) Å mean) and 'long' (1.943(6) Å mean), with the 'long' bonds in the upper ring eclipsing the 'short' bonds of the lower one. The Li–O contacts between trimeric rings are of intermediate length (1.910(5) Å mean). Within either trimeric ring the O–Li–O bond angles (mean 125.1(3)°) exceed the Li–O–Li ones (mean 114.0(2)°), the sum of angles in either trimeric ring being 717.3(3)°, indicating that both rings deviate from planarity. Each hydroxylamide
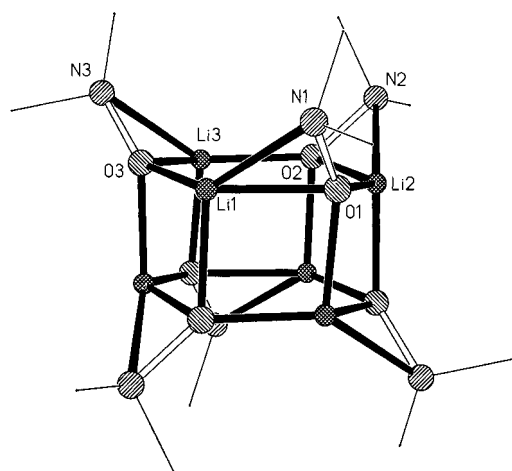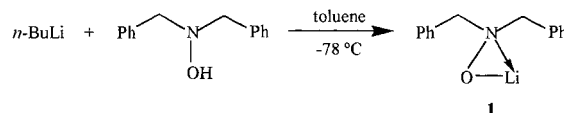
Fig. 2. The core of $\mathbf{1}_6 \cdot$ PhMe showing the two stacked Li–O trimeric rings and the staggered three-membered *N*-centre chelate rings.

Table 1
Selected bond lengths (Å) and angles (deg) for $\mathbf{1}_6 \cdot$ PhMe

Li1–O1	1.954(5)	Li1–O2a	1.926(5)
Li1–O3	1.882(6)	Li1–N1	2.100(6)
Li2–O2	1.949(6)	Li2–O3a	1.898(5)
Li2–O1	1.887(6)	Li2–N2	2.137(6)
Li3–O3	1.926(6)	Li3–O1a	1.906(5)
Li3–O2	1.879(5)	Li3–N3	2.156(6)
O1–N1	1.437(3)	N1–C1	1.478(4)
N1–C8	1.471(3)	O2–N2	1.438(3)
N2–C15	1.473(4)	N2–C22	1.467(3)
O3–N3	1.441(3)	N3–C29	1.480(4)
N3–C36	1.470(4)		
O3–Li1–O2a	96.6(2)	O3–Li1–O1	124.6(3)
O2a–Li1–O1	93.2(2)	O3–Li1–N1	135.6(3)
O2a–Li1–N1	122.0(3)	O1–Li1–N1	41.33(13)
O1–Li2–O3a	96.1(2)	O1–Li2–O2	127.7(3)
O3a–Li2–O2	95.3(2)	O1–Li2–N2	138.2(3)
O3a–Li2–N2	122.0(3)	O2–Li2–N2	40.90(13)
O2–Li3–O1a	96.2(2)	O2–Li3–O3	123.0(3)
O1a–Li3–O3	94.6(2)	O2–Li3–N3	138.4(3)
O1a–Li3–N3	119.7(3)	O3–Li3–N3	40.84(13)
N1–O1–Li2	136.4(2)	N1–O1–Li3a	138.3(2)
Li2–O1–Li3a	84.8(2)	N1–O1–Li1	74.8(2)
Li2–O1–Li1	111.4(2)	Li3a–O1–Li1	84.3(2)
O1–N1–C8	106.3(2)	O1–N1–C1	107.7(2)
C8–N1–C1	109.0(2)	O1–Nl–Li1	63.9(2)
C8–N1–Li1	118.3(2)	C1–N1–Li1	132.5(2)
N2–O2–Li3	139.1(2)	N2–O2–Li1a	135.0(2)
Li3–O2–Li1a	85.8(2)	N2–O2–Li2	76.6(2)
Li3–O2–Li2	113.6(2)	Li1a–O2–Li2	82.6(2)
O2–N2–C22	106.6(2)	O2–N2–C15	107.0(2)
C22–N2–C15	108.8(2)	O2–N2–Li2	62.5(2)
C22–N2–Li2	120.0(2)	C15–N2–Li2	131.2(2)
N3–O3–Li1	140.4(2)	N3–O3–Li2a	134.3(2)
Li1–O3–Li2a	85.1(2)	N3–O3–Li3	78.2(2)
Li1–O3–Li3	117.0(2)	Li2a–O3–Li3	83.9(2)
O3–N3–C36	106.1(2)	O3–N3–C29	107.0(2)
C36–N3–C29	108.8(2)	O3–N3–Li3	61.0(2)
C36–N3–Li3	122.8(2)	C29–N3–Li3	128.4(2)

Symmetry transformations used to generate equivalent atoms a: $-x + 1/2, -y + 1/2, -z + 1$.

Table 2
Summary of energies found from calculations based on aggregates of $[H_2NOLi]_n$ ($n = 1–4,6,8,9$) using the 6-31G basis set at the S.C.F. level. Selected aggregates have been optimised using the 6-31G* basis set at the MP2 level

n	6-31G basis set at S.C.F. level			6-31G* basis set at MP2 level			Fig. 3
	Abs. energy	ΔH_{agg} (kcal mol^{-1})	$\Delta H_{agg}/n$ (kcal mol^{-1} per monomer)	Abs. energy	ΔH_{agg} (kcal mol^{-1})	$\Delta H_{agg}/n$ (kcal mol^{-1} per monomer)	
1	−137.841142	0.0	0.0	−138.24365	0.0	0.0	a
2	−275.775004	58.2	29.1	−276.577331	56.5	28.2	b
3	−413.711073	117.7	39.2	−414.9130837	114.3	38.1	c
4	−551.621066	161.0	40.3	—	—	—	d
4	−551.632156	167.9	42.0	—	—	—	e
4	−551.660676	185.8	46.5	—	—	—	f
4	−551.664568	188.3	47.1	−553.2770724	189.8	47.5	g
6	−827.460739	259.7	43.3	—	—	—	h
6	−827.462540	260.3	43.4	—	—	—	i
6	−827.511152	290.7	48.5	—	—	—	j
6	−827.521602	297.3	49.6	—	—	—	k
6	−827.532096	303.9	50.7	—	—	—	l
6	−827.538967	308.2	51.4	−829.958346	311.5	51.9	m
8	−1103.392964	393.6	49.2	—	—	—	n
8	−1103.397447	419.2	52.4	—	—	—	o
8	−1103.398268	420.0	52.5	—	—	—	p
9	−1241.330359	472.5	52.5	—	—	—	q
9	−1241.331374	477.9	53.1	—	—	—	r

To the best of our knowledge, *N*-centre chelation of lithium has been observed in only one other hexameric system, and even then one involving more extensive, so less strained, chelate rings. Hence, in the lithium enolate of *N,N*-diethylglycinate, $Li_6[OC(OEt)=C(H)NEt_2]_6$, five-membered chelates stabilise the metal centres [4]. Nevertheless, $\mathbf{1}_6 \cdot PhMe$ represents the first observation of metal centre stabilisation by virtue of *N*-centre chelation in a lithium hydroxylamide.

The propensity of organolithium species for aggregation is a long established fact [3,5,6], and numerous experimental validations of this exist. However, such experimental structural studies can clearly be complemented by calculational ones. Accordingly, therefore, extensive theoretical investigations have been carried out on most types of lithium compound, helping to elucidate bonding, aggregation modes and geometries in both organic [7,8] and inorganic [8,9] lithium species.

As has been discussed above, a lithium-bridged N–O moiety has already been successfully modelled for monomeric lithium hydroxylamide, H_2NOLi [2]. However, having established a solid-state structure of $\mathbf{1}_6 \cdot$ PhMe, it became desirable to study the energetic favourability of aggregation and to consider whether or

Table 3
Calculated geometric parameters (distances (Å), angles (deg)) for $[H_2NOLi]_n$ vs. the mean observed values for $\mathbf{1}_6 \cdot$ PhMe. The values cited for $n = 4$ and 6 correspond to the most stable configurations at those aggregation states (i.e. staggered double stack)

	$\mathbf{1}_6 \cdot$ PhMe	n(6-31G basis set at S.C.F. level)					n(6-31G* basis set at MP2 level)				
		1	2	3	4	6	1	2	3	4	6
Li–O[a]	1.910(5)	—	—	—	1.896	1.923	—	—	—	1.918	1.945
Li–O[b]	1.943(6)	1.727	1.923	1.845	2.102	1.990	1.721	1.927	1.859	2.104	1.997
Li–O[c]	1.883(6)	—	1.778	1.739	1.893	1.856	—	1.798	1.758	1.910	1.874
Li–N	2.131(6)	1.904	1.978	2.036	2.008	2.030	1.912	1.988	2.054	2.019	2.037
Li–N–O[d]	62.5(2)	59.7	66.2	60.6	72.8	67.5	59.6	66.1	61.4	72.6	67.5
Li–O–N[d]	76.5(2)	72.1	70.3	74.0	65.9	70.4	73.4	70.7	75.9	66.2	70.4
N–Li–O[d]	41.02(13)	48.2	43.5	42.7	41.3	42.1	47.0	43.2	42.7	41.2	42.1
O–Li–O	125.1(3)[f]	—	103.0[e]	130.8[e]	99.1[f]	128.1[f]	—	106.5[e]	133.1[e]	101.8[f]	131.1[f]
Li–O–Li	114.0(2)[f]	—	77.0[e]	109.2[e]	80.7[f]	111.2[f]	—	73.5[e]	106.9[e]	78.0[f]	108.6[f]

[a] Inter-ring distance.
[b] Intra-monomer ('long') Li–O bond.
[c] Inter-monomer ('short') Li–O bond.
[d] Within each NOLi chelate.
[e] Within each $(OLi)_n$ ring.
[f] Within each $(OLi)_{n/2}$ ring.

not the observed experimental structure could be theoretically corroborated and rationalised. Calculations [10,11] based on $[H_2NOLi]_n$ ($n = 1$–4,6,8,9) were done initially using the 6-31G basis set at the S.C.F. level, thereafter the most stable geometries being optimised with the 6-31G* basis set [12] at the higher MP2 level [13]. The results clearly indicate not only that aggregate stability ΔH_{agg} increases with n, but also that as the degree of aggregation is raised so too is the stabilisation energy per monomer. However, the extent to which ΔH_{agg} increases is found to diminish as the aggregates get bigger. Energetic results are summarised in Table 2. Table 3 records structural parameters found for the optimised structures.
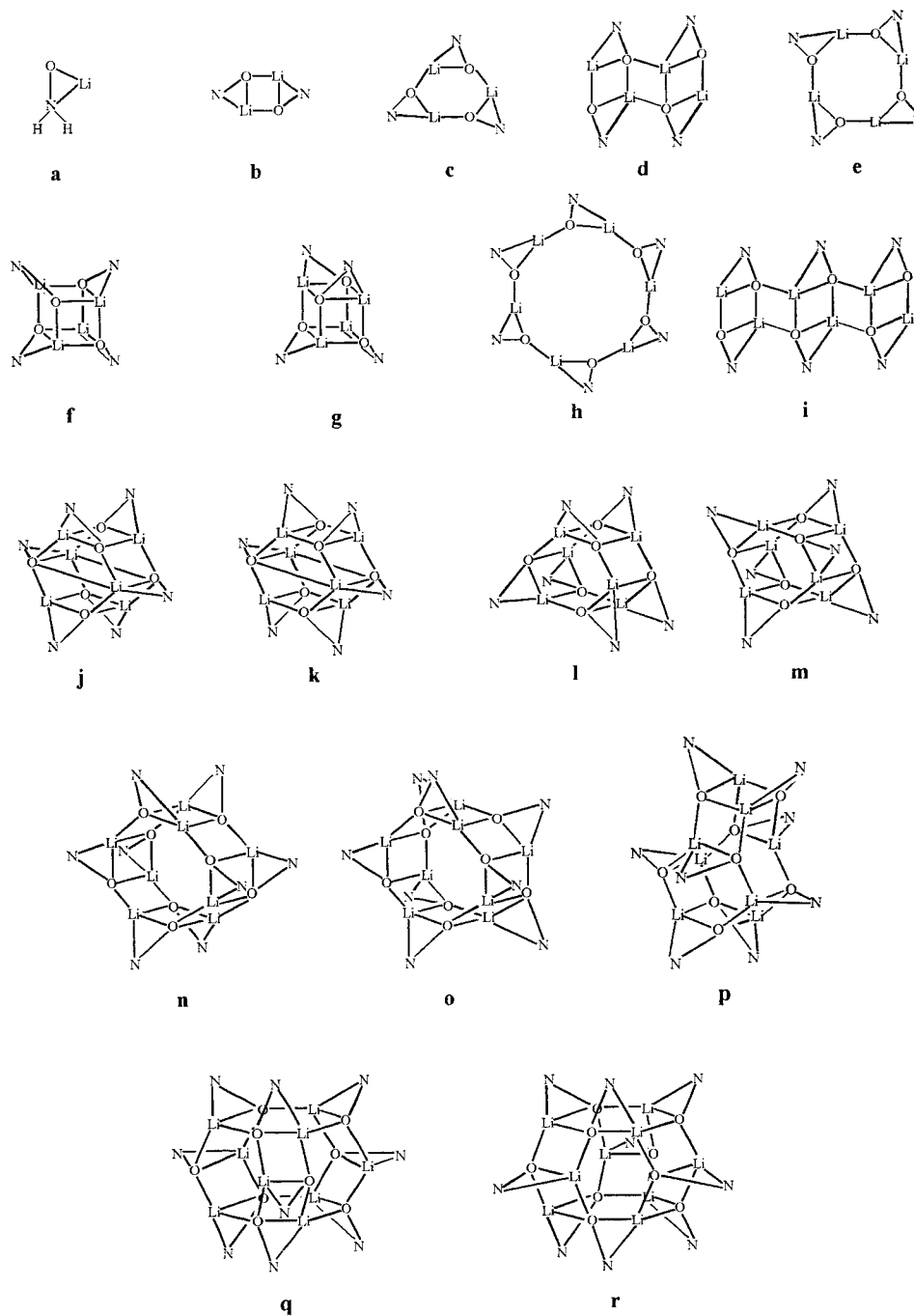

Fig. 3. Representations of optimised structures for $(H_2NOLi)_n$ ($n = 1$–4,6,8,9): (a) monomer; (b) cyclic dimer; (c) cyclic trimer; (d) ladder tetramer; (e) cyclic tetramer; (f) tetramer (eclipsed double dimer stack); (g) tetramer (staggered double dimer stack); (h) cyclic hexamer; (i) ladder hexamer; (j) hexamer (staggered triple dimer stack); (k) hexamer (eclipsed triple dimer stack); (l) hexamer (eclipsed double trimer stack); (m) hexamer (staggered double trimer stack); (n) octamer (eclipsed double tetramer stack); (o) octamer (staggered double tetramer stack); (p) octamer (staggered quadruple dimer stack); (q) nonamer (eclipsed triple trimer stack); (r) nonamer (staggered triple trimer stack).

The starting point for theoretical work is the lithium-bridged monomer (Fig. 3(a)). Interactive distances with lithium have been computed for O- and N-centres at both S.C.F. and MP2 levels, the two models demonstrating good agreement. Dimeric and trimeric aggregates have been modelled as $(LiO)_n$ planar rings at both levels (Fig. 3(b,c)). As n increases from 2 to 3, MP2 level calculations predict a lengthening of intra-monomer Li–N bonds and a concomitant shortening of intra-monomer Li–O bonds. Since the same calculations suggest that the inter-monomer Li–O bonds also shorten on going from a dimer to a trimer, it seems reasonable to suggest that increasing $(LiO)_n$ ring size from four-membered in the dimer to six-membered in the trimer yields a less strained, and thus more tightly bonded, ring system (Table 3). Both cyclic models predict that intra-monomer Li–O bonding is of a slightly lower order than inter-monomer Li–O bonding, and it seems reasonable to interpret this as a consequence of strain in the three-membered N–O–Li chelate.

For $n = 4$, calculations suggest the unsatisfactory nature of either a ladder structure or a planar ring (Fig. 3(d,e) and Table 2). Of considerably higher stability are stacked dimer cubanes, of which two types exist. Fig. 3(f) shows the eclipsed form, and Fig. 3(g) the staggered one. Lower level calculations predict that, of the two, the latter structure represents the most stable tetrameric aggregate ($\Delta H_{agg}/n = 47.1 \, kcal \, mol^{-1}$ per monomer compared with $46.5 \, kcal \, mol^{-1}$ per monomer, $1 \, kcal = 4.184 \, kJ$), presumably by virtue of minimised ligand interaction. Optimisation of the staggered structure at MP2 level indicates that both intra-monomer O–Li and N–Li bonds are lengthened ($2.104 \, Å$ and $2.019 \, Å$ respectively) relative to those observed in the cyclic dimer ($1.927 \, Å$ and $1.988 \, Å$; Table 3). The internal angles of either $(OLi)_2$ dimeric ring sum to $359.6°$, indicating essential planarity.

Hexameric aggregates have been modelled in a variety of geometries (Fig. 3(h–m)). Akin to lower level results for $n = 4$, it is found that both the cyclic (Fig. 3(h)) and ladder (Fig. 3(i)) structures are of inferior stability ($\Delta H_{agg}/n = 43.3 \, kcal \, mol^{-1}$ per monomer and $43.4 \, kcal \, mol^{-1}$ per monomer respectively at the S.C.F. level). Subsequently, several stacked hexamers have been modelled at the lower level. Fig. 3(j) and Fig. 3(k) are based on a hexameric structure which may be considered as being a triple stack of dimeric pairs or alternatively a cyclised ladder, depending upon whether or not the extended O–Li interactions which transcend either hexagonal face ($3.578 \, Å$ in Fig. 3(j) and $3.534 \, Å$ in Fig. 3(k)) are considered to be of any bonding relevance. Perhaps surprisingly, the structure depicted in Fig. 3(k) is the nominally more stable of the two, in spite of the fact that all of its N–O–Li chelates are eclipsed.

Of superior stability at the S.C.F. level are the hex-

americ structures represented in Fig. 3(l) and Fig. 3(m). These are based on a double stack of trimeric rings arranged in such a way that the metal centres of one ring lie above the oxygen centres of the other, and vice versa. The N–O–Li chelates can be arranged in a relatively eclipsed (Fig. 3(l)) or staggered (Fig. 3(m)) fashion, yielding differing aggregate stabilities both overall and per monomer (Table 2, $\Delta H_{agg}/n = 50.7 \, kcal \, mol^{-1}$ per monomer and $51.4 \, kcal \, mol^{-1}$ per monomer respectively at the S.C.F. level). That stability per monomer is optimised by staggering the hexameric double trimeric ring stacking model is unsurprising, the energetic favourability ($0.7 \, kcal \, mol^{-1}$ per monomer at the S.C.F. level) being attributable to a minimisation of the steric interactions between the $-NH_2$ moieties on either ring.

Having indicated the favourability of the staggered hexameric double $(LiO)_3$ ring stacking model at the S.C.F. level, geometry optimisation at the MP2 level has allowed us to probe more precisely the exact structural nature of this aggregate. Its staggered double stack demonstrates alternating long and short Li–O interactions within each ring, the internal angles of which sum to $718.95°$, indicating slight deviation of the six-membered rings from planarity (Fig. 4). Within either trimeric ring, the longer Li–O interactions are those involved in the three-membered chelate. These features are all entirely consistent with the solid-state structure of $\mathbf{1}_6 \cdot$ PhMe (Table 3). While the theoretical treatment yields only crude approximations to bond angles observed in the three-membered chelate, interactive distances are, on the whole, accurately predicted, though it generally appears that, within either trimeric ring, calculations correctly estimate the short, inter-monomer Li–O inter-
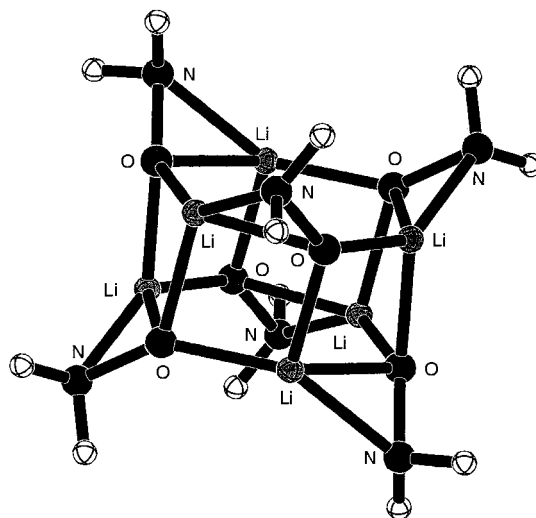

Fig. 4. The geometry-optimised Li-bridged hydroxylamide hexamer of maximum stability modelled with the 6-31G* basis set at the MP2 level, for which $\Delta H_{agg}/n = 51.9 \, kcal \, mol^{-1}$ per monomer. This is isostructural with lithium dibenzylhydroxylamide, $\mathbf{1}_6$.

action while overestimating the length of the longer (intra-monomer) one (1.997 Å at the MP2 level compares with the observed experimental mean of 1.943(6) Å). Correspondingly, it is apparent that theory tends to over-emphasise the extent of N–Li bonding, the calculated distance of 2.037 Å being rather shorter than the observed mean of 2.131(6) Å. The predicted Li–O inter-ring distance, at 1.945 Å, is greater than that observed in $\mathbf{1}_6 \cdot$ PhMe (1.910(5) Å). While this suggests that theory over-states *N*-stabilisation, mostly at the expense of intra-monomer *O*-stabilisation, it is nevertheless clear that the solid-state structure of $\mathbf{1}_6 \cdot$ PhMe shows the product in the most thermodynamically feasible supramolecular arrangement considered thus far.

Calculational studies of higher aggregates using the 6-31G basis set at the S.C.F. level indicate only rather nominal increments in stability over and above that predicted for the most stable hexamer. Three octamers have been modelled (Fig. 3(n–p)). Of these, two (Fig. 3(n) and Fig. 3(o)) represent extensions of the eclipsed and staggered double $(\text{LiO})_{n/2}$ ring stacks discussed for $n = 4$ and 6. Unsurprisingly, calculations suggest that the staggered model is the more stable of the two ($\Delta H_{\text{agg}}/n = 49.2$ kcal mol^{-1} per monomer and 52.4 kcal mol^{-1} per monomer respectively). Of slightly greater stability ($\Delta H_{\text{agg}}/n = 52.5$ kcal mol^{-1} per monomer) is the structure represented in Fig. 3(p). This is best described as four sets of dimers stacked in a staggered fashion, wherein the inter-molecular O–Li linkages of the middle two dimers have cleaved.

Finally, nonameric aggregates have been modelled, representing triple-decker extensions of the hexameric double $(\text{LiO})_3$ ring stacking model. Of the two structural models attempted for $n = 9$ (see Fig. 3(q,r)) the staggered form represents the most thermodynamically viable option by 0.6 kcal mol^{-1} per monomer. While this nonameric structure represented in Fig. 3(r) thus represents the most thermodynamically favourable model according to theory, it is nevertheless the case that, upon closer inspection of the data reported in Table 2, a more complex story evolves. It is readily apparent, even after only a superficial consideration of $\Delta H_{\text{agg}}/n$, that the increment in this value is greater for increases in aggregation state when n is small whereas it is somewhat smaller for increases in the larger values of n. Hence, for example, the transition $n = 1 \rightarrow 2$ is accompanied by a 29.1 kcal mol^{-1} per monomer increase in the value of $\Delta H_{\text{agg}}/n$, while a 10.1 kcal mol^{-1} per monomer increment is observed for $n = 2 \rightarrow 3$. However raising $n = 3$ to even the most stable tetramer yields a thermodynamic gain of only 7.9 kcal mol^{-1} per monomer. This same trend accounts for the observation that the thermodynamic gain to be had by making $n > 6$ is increasingly superficial, with calculational studies thus suggesting that $\Delta H_{\text{agg}}/n$ increases to some absolute limit.

Of course, a necessary calculational limitation is the replacement of sterically demanding ligands by simpler, and more importantly, smaller groups or atoms. In this study specifically, the benzyl groups of the experimental system $[(\text{PhCH}_2)_2\text{NOLi}]_n$ have been replaced by hydrogen atoms, calculations being performed on $(\text{H}_2\text{NOLi})_n$ aggregates. An obvious likely consequence of such ligand simplification is that calculations may over-estimate the stability of aggregates in the absence of steric factors. It seems reasonable to suggest that such overestimation will be most marked for higher and more congested aggregates. Here theory corroborates experiment (insofar as electrostatic considerations go) in that the hexamer $(\text{H}_2\text{NOLi})_6$, akin to $\mathbf{1}_6$ PhME, is more stable than lower aggregates. Nonetheless, yet higher aggregates are even more stable - but by very little: the changes in H_{agg}/n are only 1.1 and 1.7 kcal^{-1} mol^{-1} monomer^{-1} on going from $n = 6$ to $n = 8$ and from $n = 6$ to $n = 9$ respectively. It seems reasonable to suppose that these small incremental increases in the stability of higher aggregates ($n > 6$) would, in practice, be more than offset by the introduction of excessive steric hindrance into the aggregate.

In conclusion, it is clear that the first reported example of an unsolvated, self-stabilising lithium hydroxylamide, $\mathbf{1}_6 \cdot$ PhMe, in which the metal centres are tetravalent both by virtue of ring stacking and lithium-bridging of the hydroxylamide functions, can be modelled theoretically. Calculations readily demonstrate its thermodynamic favourability, both absolutely and as a function of aggregation state, indicating, as they do, the systematic depletion of incremental increase in thermodynamic stability as n rises. That a higher aggregation state is not observed, in spite of predictions of nominally enhanced stability according to theory, can be rationalised in terms of steric effects. Nevertheless, extensive calculational studies have clearly proven to be of significant utility in understanding the observed structure.

3. Experimental

3.1. General experimental

Standard inert-atmosphere Schlenk techniques were employed using a dual nitrogen/vacuum line. Schlenk tubes were pre-dried at 180°C prior to evacuation to less than 0.1 Torr three times, being filled with dry nitrogen from the house supply between each evacuation. Reagents were used as received from Aldrich Chemical Company. Dibenzylhydroxylamine was preweighed in a glove box under dry Ar gas and added directly to the Schlenk tube in the glove box. Toluene (freshly distilled and maintained at reflux over sodium)

and n-butyllithium were added direct to the nitrogen-filled Schlenk tube using standard syringe techniques.

The ^{1}H NMR spectrum of $\mathbf{1}_6 \cdot$ PhMe was recorded at room temperature using a Bruker WM 250 FT-NMR spectrometer.

3.2. Preparation of $[(PhCH_2)_2NOLi]_6 \cdot PhMe$, $\mathbf{1}_6 \cdot PhMe$

To a solution of dibenzylhydroxylamine (2.13 g, 10 mmol) in 7 ml toluene at $-78\,^\circ$C was added n-butyllithium (6.25 ml, 10 mmol, 1.6 M in hexanes). Warming the resultant yellow solution to room temperature gave a pink suspension, which afforded a red solution on gentle heating. Storage at $+5\,^\circ$C for 3 days afforded colourless crystals of $[(PhCH_2)_2NOLi]_6 \cdot$ PhMe, $\mathbf{1}_6 \cdot$ PhMe, m.p., 175–177 $^\circ$C, yield, 51%. Found, C 76.3, H 6.6, N 5.8. Calcd. for $C_{91}H_{92}Li_6N_6O_6$, C 77.7, H 6.4, N 6.4. ^{1}H NMR spectroscopy (250 MHz, 25 $^\circ$C, C_6D_6), δ 2.07 (s, 0.41H, toluene), 3.56 (s, br, 4H, CH_2), 7.04 (m, 0.68H, toluene), 7.17 (m, 2H, p-Ph), 7.29 (t, 4H, m-Ph), 7.44 (d, 4H, o-Ph).

3.3. X-ray crystallography

Crystal data for $\mathbf{1}_6 \cdot$ PhMe: $C_{84}H_{84}Li_6N_6O_6 \cdot C_7H_8$, $M_r = 1407.4$, monoclinic, space group $C2/c$, $a = 23.893(4)$, $b = 16.718(3)$, $c = 20.970(4)$ Å, $\beta = 102.94(2)^\circ$, $V = 8164(3)$ Å^3, $Z = 4$ $D_c = 1.145$ g cm^{-3}, $\mu = 0.55$ mm^{-1} for Cu Kα radiation ($\lambda = 1.54184$ Å), $F(000) = 2984$, $T = 295$ K. Unit cell parameters were refined from 2θ values (30–40°) of 32 reflections measured at $\pm\omega$ on a Stoe–Siemens diffractometer. Intensities were measured with $\omega-\theta$ scans and an on-line profile fitting procedure [14], from a crystal of size $0.3 \times 0.2 \times 0.2$ mm^3. Corrections were made for 3.5% decay in the intensities of periodically monitored standard reflections, but not for absorption. The structure was determined by direct methods [15] and refined on F^2 by full-matrix least squares methods from 5141 independent reflections ($2\theta \leq 110^\circ$, 9497 reflections measured, $R_{int} = 0.0306$), with a weighting scheme $w^{-1} = \sigma^2(F_o^2) + (0.0528P)^2 + 4.2028P$, where $P = (F_o^2 + 2F_c^2)/3$. Hydrogen atoms were included with a riding model, and other atoms were refined with anisotropic displacement parameters. An isotropic extinction parameter x was refined to 0.00032(3), whereby $F_c' = F_c/(1 + 0.001\,xF_c^2\lambda^3/\sin 2\theta)^{+1/4}$. The methyl group of the toluene solvent molecule is equally disordered over two sites and no hydrogen atoms were included. All shift/E.S.D. ratios were < 0.001 in the final refinement cycle. For all reflections, $R_w = \Sigma[w(F_o^2 + F_c^2)^2]/S[w(F_o^2)^2]^{1/2} = 0.1474$; the conventional $R = 0.0457$ for F values of 3022 reflections with $F_o^2 > 2\sigma(F_o^2)$; goodness of fit = 1.089 on F^2 values for all data and 498 refined parameters. All features in a final

Table 4
Atomic coordinates ($\times 10^4$) and equivalent isotropic displacement parameters (Å$^2 \times 10^3$) for $\mathbf{1}_6 \cdot$ PhMe

	x	y	z	U_{eq}
Li1	2817(2)	2939(3)	5931(3)	66.3(14)
Li2	3168(2)	2656(3)	4576(3)	67.4(14)
Li3	1928(2)	3393(3)	4568(3)	67.2(14)
O1	3426.8(8)	2633.9(11)	5494.0(9)	62.3(5)
N1	3689.7(11)	3189.3(14)	5995.1(11)	60.3(7)
C1	4223.2(14)	2818(2)	6373(2)	72.7(9)
C2	4118.2(14)	2174(2)	6835(2)	71.8(9)
C3	4018(2)	1393(2)	6638(2)	86.1(11)
C4	3910(2)	806(3)	7059(3)	108.2(14)
C5	3905(2)	1006(3)	7687(3)	119(2)
C6	4008(2)	1772(3)	7897(2)	123(2)
C7	4117(2)	2360(2)	7473(2)	94.8(12)
C8	3838.9(14)	3900(2)	5654.4(15)	68.9(9)
C9	3904.1(14)	4657(2)	6041(2)	68.4(9)
C10	3828(2)	4708(2)	6667(2)	97.8(12)
C11	3857(2)	5452(3)	6979(3)	132(2)
C12	3962(2)	6129(3)	6659(3)	140(2)
C13	4035(2)	6083(2)	6041(3)	120(2)
C14	4009(2)	5355(2)	5736(2)	88.6(11)
O2	2465.7(8)	3139.4(11)	4067.9(9)	64.3(6)
N2	2911.2(10)	3524.0(14)	3818.6(11)	61.2(7)
C15	2757.5(15)	3440(2)	3101.3(15)	75.2(9)
C16	2830.5(15)	2614(2)	2863.4(14)	70.3(9)
C17	2387(2)	2068(3)	2759(2)	82.5(10)
C18	2453(2)	1300(3)	2539(2)	98.8(12)
C19	2966(2)	1074(3)	2412(2)	109.2(14)
C20	3413(2)	1603(3)	2508(2)	105.0(13)
C21	3347(2)	2365(2)	2734(2)	87.0(11)
C22	2894.7(14)	4374(2)	3985(2)	68.8(9)
C23	3418.0(15)	4842(2)	3924.9(15)	68.9(9)
C24	3930(2)	4481(2)	3908(2)	95.2(12)
C25	4412(2)	4934(3)	3876(2)	123(2)
C26	4375(3)	5756(4)	3869(3)	130(2)
C27	3872(3)	6107(3)	3894(2)	119(2)
C28	3398(2)	5662(2)	3919(2)	89.3(11)
O3	2115.8(9)	3408.4(11)	5510.1(9)	64.7(6)
N3	1858.4(10)	4184.5(14)	5358.2(12)	61.1(7)
C29	1384.6(14)	4248(2)	5705(2)	71.1(9)
C30	856.7(14)	3786(2)	5394(2)	67.1(9)
C31	449(2)	4129(2)	4906(2)	87.4(11)
C32	−56(2)	3728(3)	4632(2)	108.5(14)
C33	−146(2)	2976(3)	4841(3)	110.3(15)
C34	256(2)	2621(3)	5320(2)	101.6(13)
C35	755(2)	3029(2)	5601(2)	80.0(10)
C36	2304.6(14)	4770(2)	5638(2)	70.3(9)
C37	2124.2(15)	5624(2)	5473(2)	73.6(9)
C38	2219(2)	6204(2)	5955(2)	99.3(12)
C39	2079(2)	6995(2)	5812(3)	129(2)
C40	1848(2)	7213(3)	5196(4)	132(2)
C41	1745(2)	6653(3)	4700(3)	127(2)
C42	1887(2)	5855(2)	4848(2)	104.2(13)
C43	0	2656(5)	7500	137(3)
C44	−88(2)	3064(4)	6929(3)	131(2)
C45	−96(2)	3873(4)	6921(4)	152(3)
C46	0	4296(6)	7500	176(5)
C47	−171(4)	4412(6)	6434(4)	129(3)

U_{eq} is defined as one-third of the trace of the orthogonalised U_{ij} tensor.

difference synthesis lie between $+0.13$ and $-0.13\,e^-\,\mathring{A}^{+3}$.

Atomic displacement parameters, hydrogen atom coordinates, and complete geometry have been deposited at the Cambridge Crystallographic Data Centre. Non-hydrogen atom coordinates and equivalent isotropic displacement parameters are given in Table 4.

3.4. Theoretical analysis

Ab initio calculations using the GAMESS [10] and GAUSSIAN 94 [11] computer programs were done on $[H_2NOLi]_n$ ($n = 1$–4,6,8,9); initially the 6-31G basis set [12] at the S.C.F. level was used and thereafter the most stable geometries up to and including the hexamer were re-optimised with the 6-31G* basis set [12] at the higher MP2 level [13] using the frozen core (FC) option.

Acknowledgements

References

[1] G. Boche, H.-U. Wagner, J. Chem. Soc. Chem. Commun. (1984) 1591.

[2] D.R. Armstrong, R. Snaith, G.T. Walker, J. Chem. Soc. Chem. Commun. (1985) 789.

[3] (a) W. Setzer, P.v.R. Schleyer, Adv. Organomet. Chem. 24 (1985) 353. (b) D. Seebach, Angew. Chem. Int. Edn. Engl. 27 (1988) 1624. (c) R.E. Mulvey, Chem. Soc. Rev. 20 (1991) 167. (d) K. Gregory, P.v.R. Schleyer, R. Snaith, Adv. Inorg. Chem. 37 (1991) 47.

[4] J.T.B.H. Jastrzebski, G. van Koten, W.F. van de Mieroop, Inorg. Chem. Acta 142 (1988) 169.

[5] G. Boche, J.C.W. Lohrenz, in: A.-M. Sapse, P.v.R. Schleyer (Eds.), Lithium Chemistry: A Theoretical and Structural Overview, Wiley, New York, 1995, Chapter 7 and references cited therein.

[6] F. Pauer, P.P. Power, in: A.-M. Sapse, P.v.R. Schleyer (Eds.), Lithium Chemistry: A Theoretical and Structural Overview, Wiley, New York, 1995, Chapter 9 and references cited therein.

[7] A. Streitwieser, S.M. Bachrach, A. Dorigo, P.v.R. Schleyer, in: A.-M. Sapse, P.v.R. Schleyer (Eds.), Lithium Chemistry: A Theoretical and Structural Overview, Wiley, New York, 1995, Chapter 1 and references cited therein.

[8] A.-M. Sapse, D.C. Jain, K. Raghavachari, in: A.-M. Sapse, P.v.R. Schleyer (Eds.), Lithium Chemistry: A Theoretical and Structural Overview, Wiley, New York, 1995, Chapter 2 and references cited therein.

[9] R. Snaith, D.S. Wright, in: A.-M. Sapse, P.v.R. Schleyer (Eds.), Lithium Chemistry: A Theoretical and Structural Overview, Wiley, New York, 1995, Chapter 8 and references cited therein.

[10] (a) M. Dupuis, D. Spangler, J.J. Wendoloski, GAMESS NRCC Software Catalogue, Program No. 2 GOI, 1980, vol. 1. (b) M.F. Guest, J. Kendrick, S.A. Pope, GAMESS Documentation, Daresbury Laboratory, Warrington, UK, 1983. (c) M.F. Guest, P. Fantucci, R.J. Harrison, J. Kendrick, J.H. van Lenthe, K. Schoeffel, P. Sherwood, GAMESS-UK, Daresbury (CFS Ltd. 1993).

[11] M.J. Frisch, G.W. Trucks, H.B. Schlegel, P.M.W. Gill, B.G. Johnson, M.A. Robb, J.R. Cheeseman, T. Keith, G.A. Petersson, J.A. Montgomery, K. Raghavachari, M.A. Al-Laham, V.G. Zakrzewski, J.V. Ortiz, J.B. Foresman, J. Cioslowski, B.B. Stefanov, A. Nanayakkara, M. Challacombe, C.Y. Peng, P.Y. Ayala, W. Chen, M.W. Wong, J.L. Andres, E.S. Replogle, G. Gomperts, R.L. Martin, D.J. Fox, J.S. Brinkley, D.J. Defrees, J. Baker, J.J.P. Stewart, M. Head-Gordon, C. Gonzalez, J.A. Pople, GAUSSIAN 94 Revision C.3, Gaussian, Inc., Pittsburgh. PA, 1995.

[12] (a) W.J. ehre, R. Ditchfield, J.A. Pople, J. Chem. Phys. 56 (1972) 2257. (b) P.C. Hariharan, J.A. Pople, Theor. Chim. Acta 28 (1973) 213. (c) J.D. Dill, J.A. Pople, J. Chem. Phys. 62 (1975) 618.

[13] C. Moller, M.S. Plesset, Phys. Rev. 46 (1934) 618.

[14] W. Clegg, Acta Crystallogr. Sect. C: 37 (1981) 22.

[15] G.M. Sheldrick, SHELXTL user manual, version 5, Siemens Analytical X-ray Instruments Inc., Madison, WI, USA, 1994.